LAWRENCE
LIVERMORE
NATIONAL
LABORATORY

LLNL-JRNL-819629

The Reflection of a Blast Wave by a Very Intense Explosion I. Scaling and Similarity

A. Cook, J. Bauer, M. Cook, G. Spriggs

February 18, 2021

The Reflection of a Blast Wave by a Very Intense Explosion

Disclaimer

PROCEEDINGS A

rspa.royalsocietypublishing.org

Research

Article submitted to journal

Subject Areas:
Nuclear Weapons Testing, Euler Equations, Similarity Solutions

Keywords:
Blast Waves, Numerical Simulations

Author for correspondence:
Insert corresponding author name
e-mail: awcook@llnl.gov

The Reflection of a Blast Wave by a Very Intense Explosion I. Scaling and Similarity

Andrew W. Cook[1], Joseph D. Bauer[1] and Gregory D. Spriggs[1]

[1]Lawrence Livermore National Laboratory

We demonstrate that the geometric similarity of Taylor's blast wave persists beyond reflection from an ideal surface. Upon impacting the surface, the spherical symmetry of the blast wave is lost but its cylindrical symmetry endures. As the flow acquires dependence on a second spatial dimension, an analytic solution of the Euler equations becomes elusive. However, the preservation of axisymmetry, geometric similarity and planar symmetry in the presence of a mirror-like surface causes all flow solutions to collapse when scaled by the height of burst (HOB) and the shock arrival time at the surface. The scaled blast volume for any yield, HOB and ambient air density follows a single universal trajectory for all scaled time, both before and after reflection.

THE ROYAL SOCIETY PUBLISHING

LLNL-JRNL-819629

Nomenclature

Indicators

$[=]$	"has units of"
$\mathcal{L}$	denotes units of length
$\mathcal{M}$	denotes units of mass
$\mathcal{T}$	denotes units of time

Constants

γ	adiabatic index of air, aka ratio of specific heats
ρ_a	ambient air density at burst location
H	height of burst (HOB)
S_γ	Taylor's similarity constant
t_H	time when blast contacts surface
V_H	blast volume at t_H
Y	total energy-yield of device
Y_a	portion of total yield that couples to air and forms blast wave
Y_l	portion of total yield "lost" to radiation, vaporization of bomb material etc.

Variables

Ω	geometric parameter
Ψ	reflection function
ρ	density
Θ	reflected-energy parameter
e	internal energy
p	pressure
R_s	spherical blast radius according to Taylor's solution
t	time since detonation
V	blast volume

1. Introduction

The Taylor [1, 2], von Neumann [3] and Sedov [4] solutions for a self-similar blast wave in the strong-shock limit have been used for eight decades to estimate the yields of nuclear tests and to explain the behaviour of supernovae [5], stellar wind bubbles [6], and other high-energy phenomena that produce strong shockwaves [7, 8]. During the atmospheric-testing era, weapon scientists employed Taylor's equation to estimate the yields of 210 atmospheric tests by analyzing high-speed camera films [9, 10]. In most of these tests, the devices were detonated sufficiently high above the ground to ignore the shock interaction with the surface. In fourteen events, however, the blast wave's interaction with the ground altered its rate of expansion. The measured blast distances in these cases appear to exceed Taylor's prediction due to reflected energy reinforcing the upward-moving shock. Consequently, their yields appear to be up to 40% higher than the yields determined by radiochemical techniques, light-curve analyses and other methods.

The Mohawk event, for example, exhibited a large discrepancy in the yield inferred by Edgerton, Germeshausen and Grier, Inc. (EG&G), when comparing the blast volume to the light output; i.e., the blast volume suggested a yield of ~ 360 kilotons whereas the light output indicated ~ 248 kilotons [11]. EG&G reasoned that spots on the fireball surface and the appearance of a bulbous jet, seen in Fig. 1, corrupted the light measurements; hence they rejected the light-curve data and reported the higher yield. EG&G, however, did not account for the reflection of the blast wave from the ground surface, which significantly increased the blast volume. The purpose of this paper is to lay out the additional reflection equations, which must be applied to film data in order to properly account for reflected blast energy.

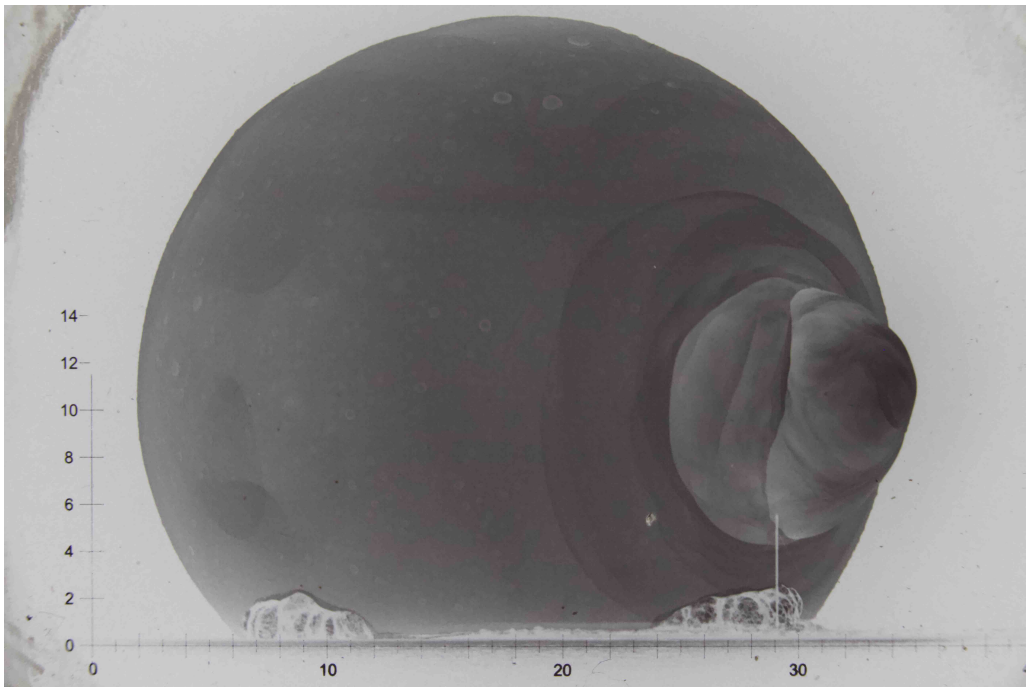

Figure 1. The Mohawk event at t=0.010148 s. The bulbous jet on the right was caused by shielding placed alongside the device.

2. Dimensional Analysis

Taylor's blast wave [1, 2] for air with zero ambient energy and pressure is governed by only two parameters possessing physical dimensions; the energy of the point source

$$Y_a[=]\frac{\mathcal{M}\mathcal{L}^2}{\mathcal{T}^2} \tag{2.1}$$

and the density of the air into which the energy is deposited

$$\rho_a[=]\frac{\mathcal{M}}{\mathcal{L}^3} \tag{2.2}$$

Combining Y_a and ρ_a to eliminate $\mathcal{M}$ results in a single fixed relation between $\mathcal{L}$ and $\mathcal{T}$. In Taylor's infinite atmosphere, where no intrinsic length or time scales exist, $\mathcal{L}$ and $\mathcal{T}$ remain locked together ($\mathcal{L}^5 \propto \mathcal{T}^2$), such that neither can abide independent of the other. The blast radius must therefore scale with its own time of propagation,

$$R_s = S_\gamma \left(\frac{Y_a t^2}{\rho_a}\right)^{1/5} \tag{2.3}$$

where the similarity constant S_γ is solely a function of γ. The fixed relation between $\mathcal{L}$ and $\mathcal{T}$ means that the blast wave is completely specified either by its radius or time of propagation.

The presence of a boundary introduces a third dimensional parameter into the system, $H[=]\mathcal{L}$, along with a time scale, $t_H[=]\mathcal{T}$ associated with the new parameter. For a detonation at distance H above a perfectly reflecting (mirror-like) surface, the blast wave will reach the surface at time

$$t_H = \left[\frac{\rho_a}{Y_a}\left(\frac{H}{S_\gamma}\right)^5\right]^{1/2} \tag{2.4}$$

For $t > t_H$, the fixed relation between $\mathcal{L}$ and $\mathcal{T}$ is broken, the spherical symmetry is lost and R_s ceases to parameterize the flow. However, the flow remains axisymmetric and the blast can still be fully characterized by its net volume, regardless of the complexity of the Mach stem and triple point emerging from the reflection. Since the ideal surface acts as a plane of symmetry, the flow behaves as if there were two identical blasts, separated a distance $2H$ apart; i.e., a blast and its mirror image [12].

Prior to reflection, the blast volume can be written in terms of (2.3)

$$V(t \le t_H) = \frac{4\pi}{3} R_s^3 = \frac{4\pi}{3} S_\gamma^3 \left(\frac{Y_a t^2}{\rho_a} \right)^{3/5} \tag{2.5}$$

For $t/t_H > 1$, the blast gradually transforms from a sphere into a hemisphere, as energy is redirected back up from the surface. In the long-time limit, all of the blast energy is contained in a hemispherical volume. This long-term hemispherical volume, containing energy Y_a could also have arisen from an unbounded Taylor blast of energy $2Y_a$. Therefore, we can write the long-term solution as

$$V(t \gg t_H) = \frac{2\pi}{3} S_\gamma^3 \left(\frac{2Y_a t^2}{\rho_a} \right)^{3/5} \tag{2.6}$$

Comparing (2.5) to (2.6), we see that a general solution takes the form

$$V(t) = \frac{4\pi}{3\Omega} S_\gamma^3 \left(\frac{\Theta Y_a t^2}{\rho_a} \right)^{3/5} \tag{2.7}$$

where

$$\Omega\,,\ \Theta = \begin{cases} 1 \ \text{ for } \ 0 \le t/t_H \le 1 \\ 2 \ \text{ for } \ t/t_H \to \infty \end{cases} \tag{2.8}$$

Here we have introduced Ω to parameterize the geometric transformation of the blast from a sphere into a hemisphere, implicitly embedding all the intermediate complexities of the Mach stem and triple point associated with the shock-boundary interaction. The Θ parameter accounts for the energy reflected from the surface, including the time it takes for this energy to propagate back through the blast region and reach the perimeter. Since Ω and Θ obey the same limits, it is convenient to combine them into a single parameter

$$\frac{\Theta^{3/5}}{\Omega} \equiv \Psi^{-2/5} \tag{2.9}$$

At $t = t_H$, the blast volume is

$$V_H = \frac{4}{3}\pi H^3 = \frac{4}{3}\pi S_\gamma^3 \left(\frac{Y_a t_H^2}{\rho_a} \right)^{3/5} \tag{2.10}$$

and all reflections begin from the same nondimensional initial conditions: $V/V_H = 1$ at $t/t_H = 1$. Subsequently, all flows, regardless of yield, height of burst and/or ambient density, remain indistinguishable in nondimensional variables. The collapse of flow solutions is a consequence of the fact that there is nothing in the initial conditions, boundary conditions or the equations themselves to break the symmetry or geometric similarity of the blast wave; hence, the temporal evolution of V/V_H does not depend on the shape of the blast wave. Dividing (2.7) by (2.10), we obtain a universal relation between time and volume

$$\frac{V}{V_H} = \Psi^{-2/5} \left(\frac{t}{t_H} \right)^{6/5} \tag{2.11}$$

The goal of this paper is to determine Ψ by performing computer simulations to directly calculate V.

3. Numerical Simulations

We have computed Ψ numerically using the Miranda code [13] to solve the governing Euler equations [14] for the transport of mass, momentum and energy. The Miranda code discretizes spatial derivatives with a tenth-order compact-finite-difference scheme [15] and temporally integrates the equations with a fourth-order Runge-Kutta method [16]. Eighth order hyperviscosity [17] and hyperconductivity [18] are employed, along with eighth-order spectral-like dealiasing for shock capturing [19]. The blast volume is computed by tagging grid cells as the shock passes through them and then adding up the volumes of all the tagged cells.

The ideal-gas law assumed by Taylor and employed in our simulations is

$$p = (\gamma - 1)\rho e \tag{3.1}$$

In all of our simulations, we set $\gamma = 1.2265$, for which $S_\gamma = 0.91952432$. We chose this value of gamma as a best fit to blast waves analyzed in 43 atmospheric tests, including both tower shots and air bursts; i.e., we found this value to produce the best overall agreement between yields estimated from blast-wave measurements and radio-chemical methods. Before collecting results, we first verified that Miranda agrees with Taylor's solution, given sufficient grid resolution. Here we present our grid-converged results obtained at a mesh spacing of $H/800$. Simulation vs. theory for our benchmark case is displayed in Figure 2.

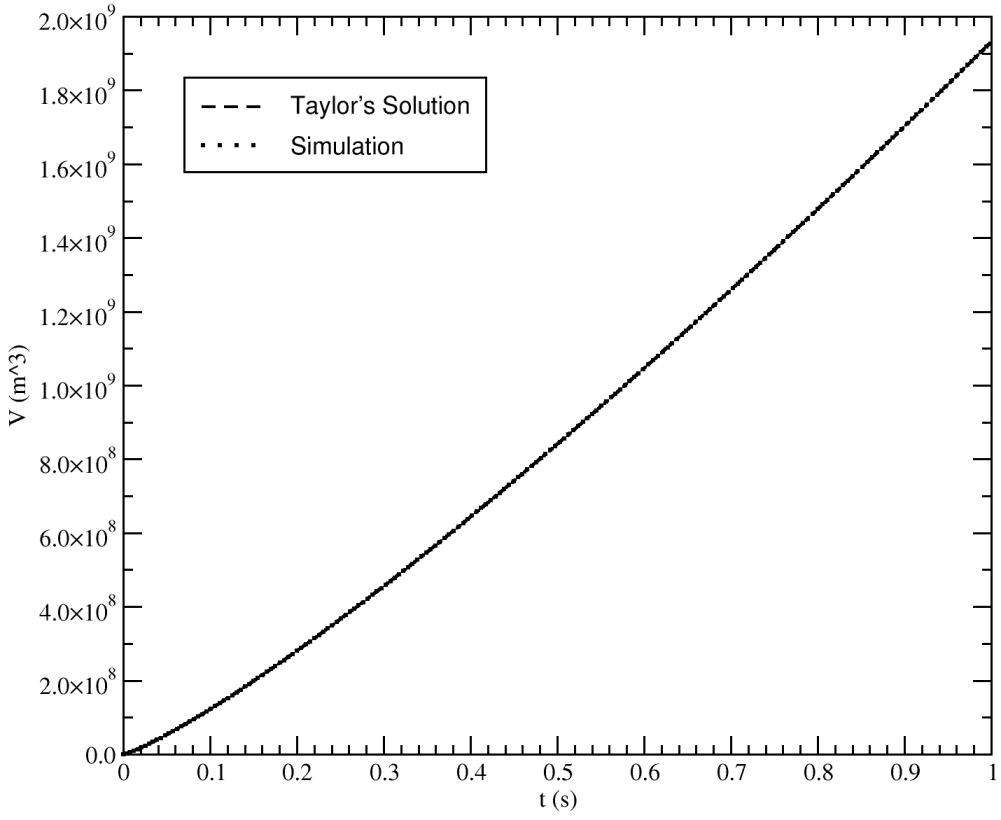

Figure 2. Blast volume vs. time for a $100\,kt$ detonation at $100\,m$ HOB in a $1\,kg/m^3$ density atmosphere.

4. Results

A useful means for comparing different cases is obtained by integrating (3.1) over all space

$$\int_{\mathbb{R}^3} p\, dV = (\gamma - 1) Y_a \tag{4.1}$$

Since pressure becomes uniformly distributed at a sufficient distance behind the blast, the nondimensional pressure, pV/Y_a, provides a natural measure of correlation for our various simulations. Figure 3 displays the nondimensional pressure from two different simulations, one at a height of burst of 10 meters and the other at an HOB of 1 kilometer. In nondimensional

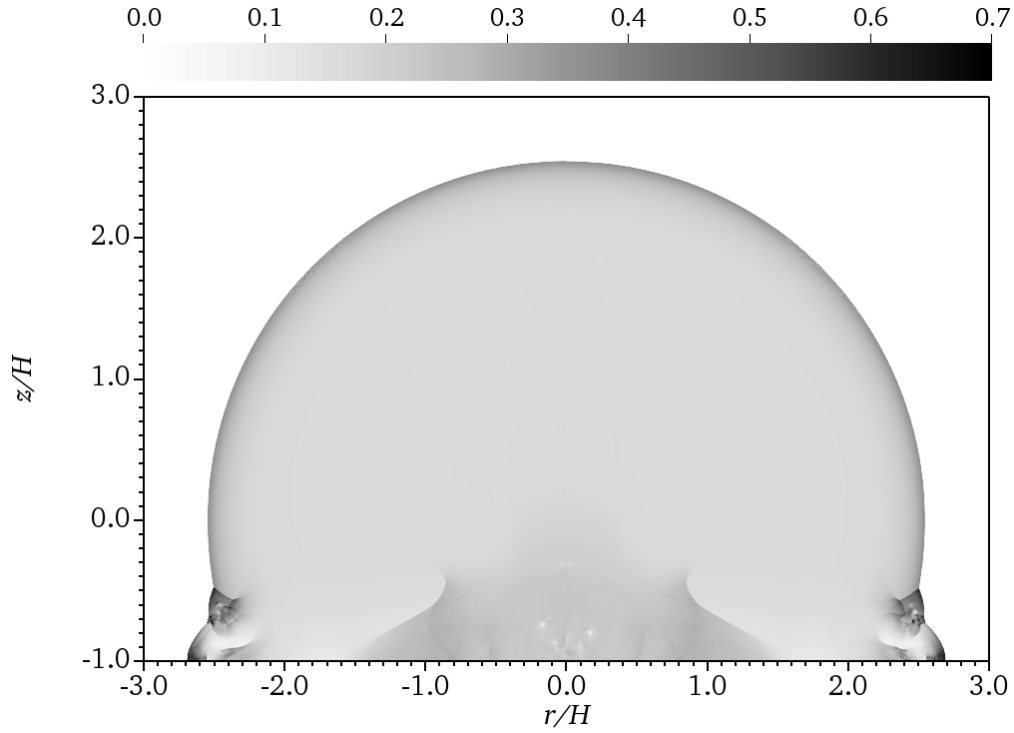

Figure 3. Nondimensional pressure at $t/t_H = 10$ for a $100\,kt$ detonation at $10\,m$ HOB (left) vs. $1\,km$ HOB (right).

coordinates, the two blasts are seen to be identical, except for tiny differences arising from grid-seeded perturbations of the vorticity field. As the shock strikes the surface at an angle, it generates baroclinic vorticity, which in turn becomes Kelvin-Helmholtz unstable, leading to the formation of vortices with low-pressure cores, seen in the image near ground zero. The perturbations to the vorticity strip are generated by the numerical discretization but the subsequent evolution of the vorticies is physical. The volume of the blast, however, is unaffected by these details.

In Figure 4 we plot scaled volume vs. scaled time for a 100 kiloton detonation at three different HOBs spanning two orders of magnitude. The nondimensionalized blast volumes are seen to collapse to a single curve. This is not too surprising, since we chose our reference time and volume to guarantee that all curves would pass through $V/V_H = 1$ at $t/t_H = 1$; i.e., changing the HOB can make no difference if time and volume are measured in HOB units.

In Figure 5 we compare different yields at the same HOB. Once again the blasts appear identical, even though the yields differ by two orders of magnitude. Changes in yield correspond to changes is blast velocity, but all velocities become equal in the chosen units, thus removing differences

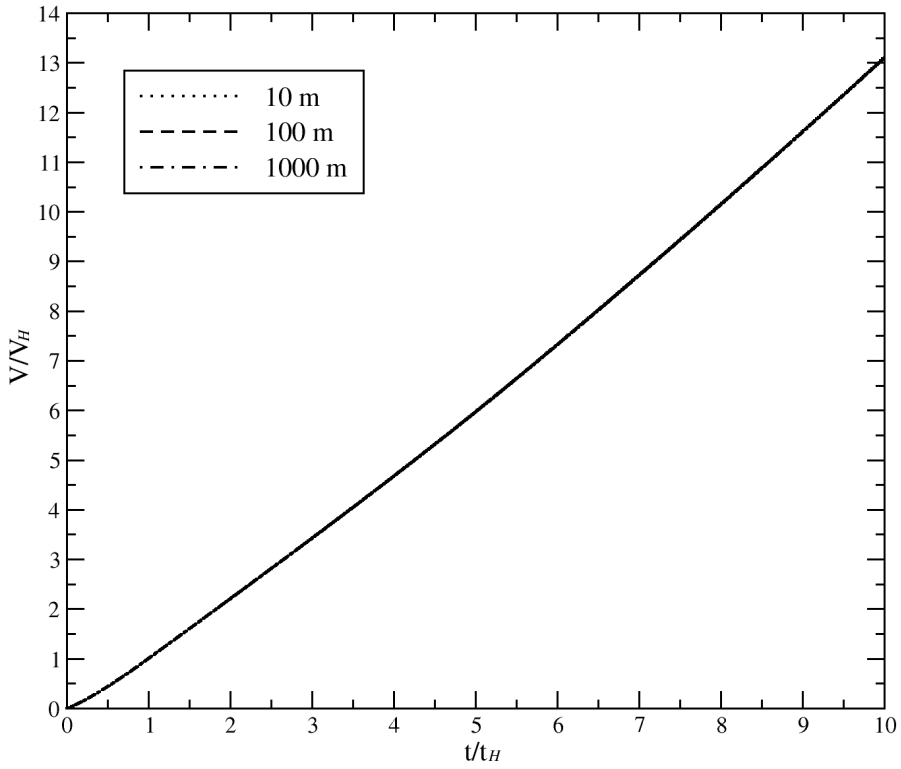

Figure 4. Nondimensional volume vs. nondimensional time for a $100\,kt$ detonation at 10, 100 and $1000\,m$ HOB.

due to yield. Tiny variations are observed once more in the vortex cores near ground zero but they do not influence the blast volume. Scaled volume vs. scaled time for three different yields is shown in Figure 6. This single collapsed curve is identical to the one in Figure 4. Although the yields and HOBs were varied in the simulations, they nevertheless all correspond to the same nondimensional case.

Finally, we varied the background density as an additional test of the theory. Figure 7 compares two simulations with atmospheric densities differing by two orders of magnitude, roughly one tenth of an atmosphere to ten atmospheres. The blasts appear identical, as they did with changes in yield and HOB. The volume vs. time curves for three background densities are displayed in Figure 8. The collapsed curve matches the previous cases.

We have thus far demonstrated that for any given yield, HOB and air density, the blast volume is a predictable function of time. In our simulations, the yield is a known input and the blast volume is calculated, however in applications of interest this process is reversed; i.e., the blast volume is measured and used to infer the yield. This becomes a straightforward procedure once the fixed relation between scaled volume and scaled time is established. Solving (2.11) for Ψ, we plot the result for all simulations in Figure 9. The undulations in the curve are due to the Mach stem and triple point working their way up the side of the blast wave. The curve fit has a correlation coefficient of 0.999345, an RMS relative error of 0.00481881 and a maximum relative error of 0.00756.

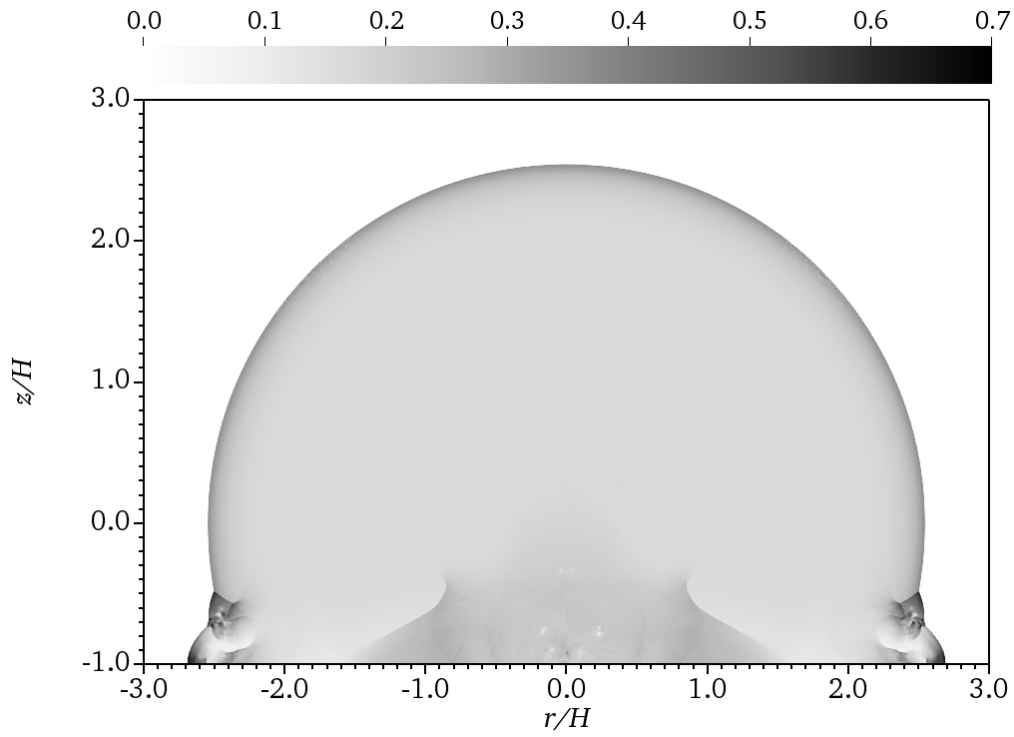

Figure 5. Nondimensional pressure at $t/t_H = 10$ for a $10\,kt$ detonation (left) vs. a $1\,Mt$ detonation (right) at $100\,m$ HOB.

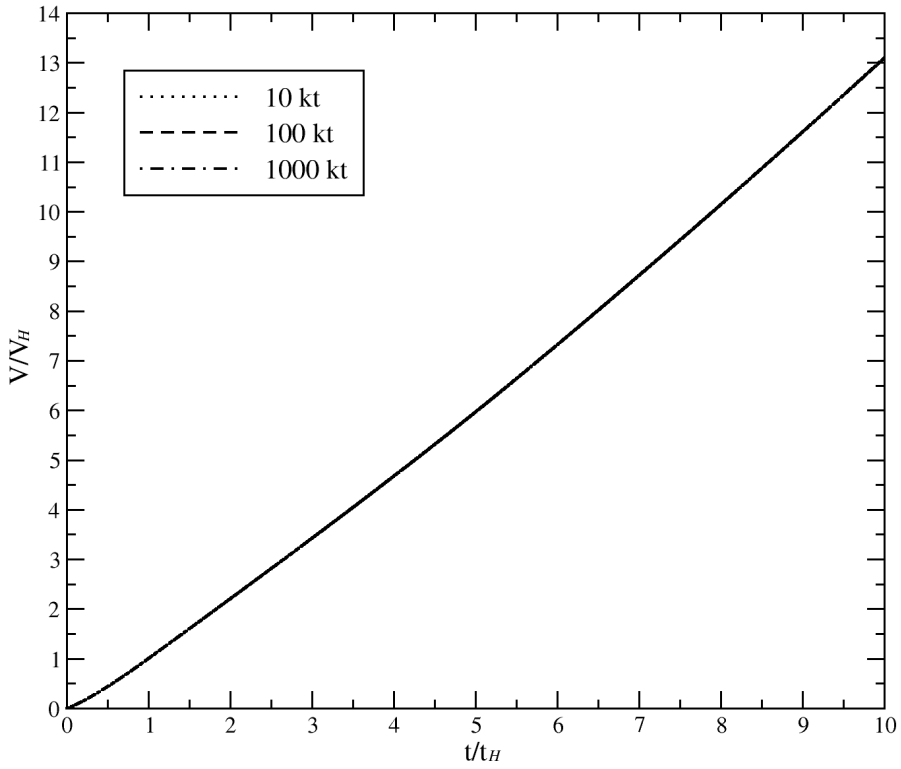

Figure 6. Nondimensional volume vs. nondimensional time for $10\,kt$, $100\,kt$ and $1\,Mt$ detonations at $100\,m$ HOB.

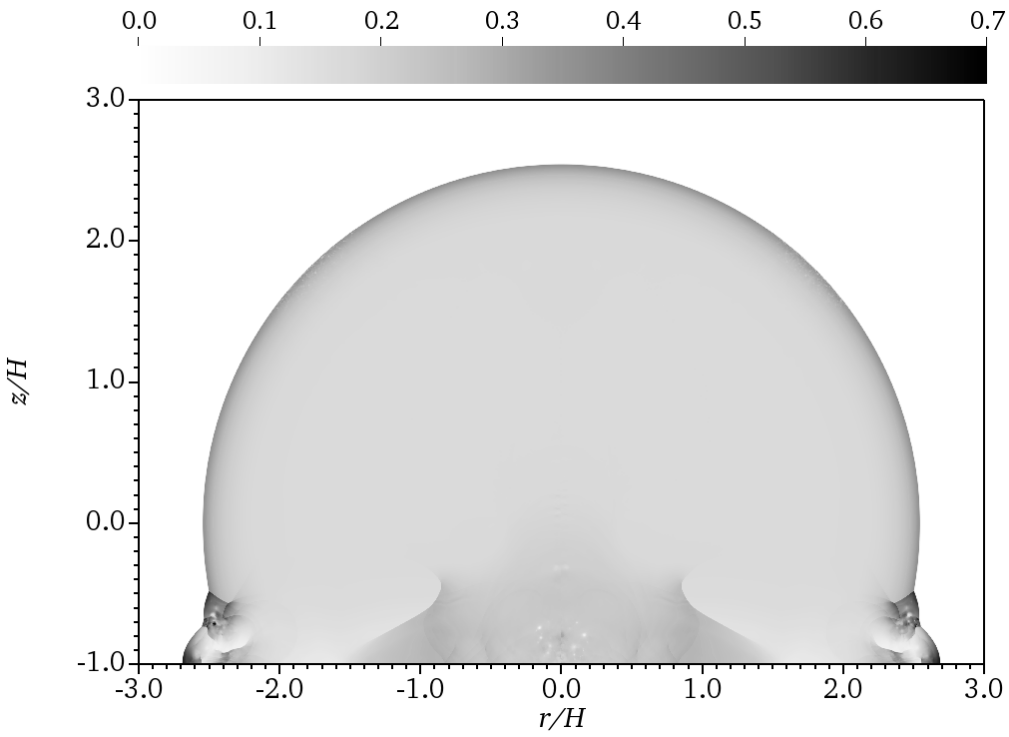

Figure 7. Nondimensional pressure at $t/t_H = 10$ for a $100\,kt$ detonation at $100\,m$ HOB with ambient density $0.1\,kg/m^3$ (left) vs. $10\,kg/m^3$ (right).

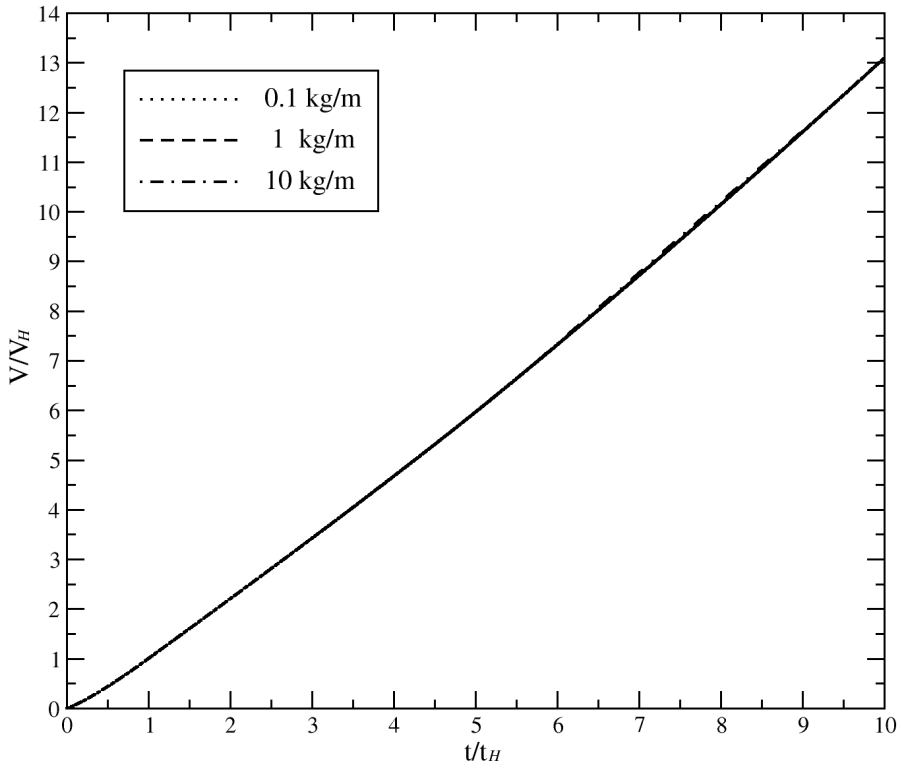

Figure 8. Nondimensional volume vs. nondimensional time for a $100\,kt$ detonation at $100\,m$ HOB with ambient densities $0.1\,kg/m^3$, $1\,kg/m^3$ and $10\,kg/m^3$.

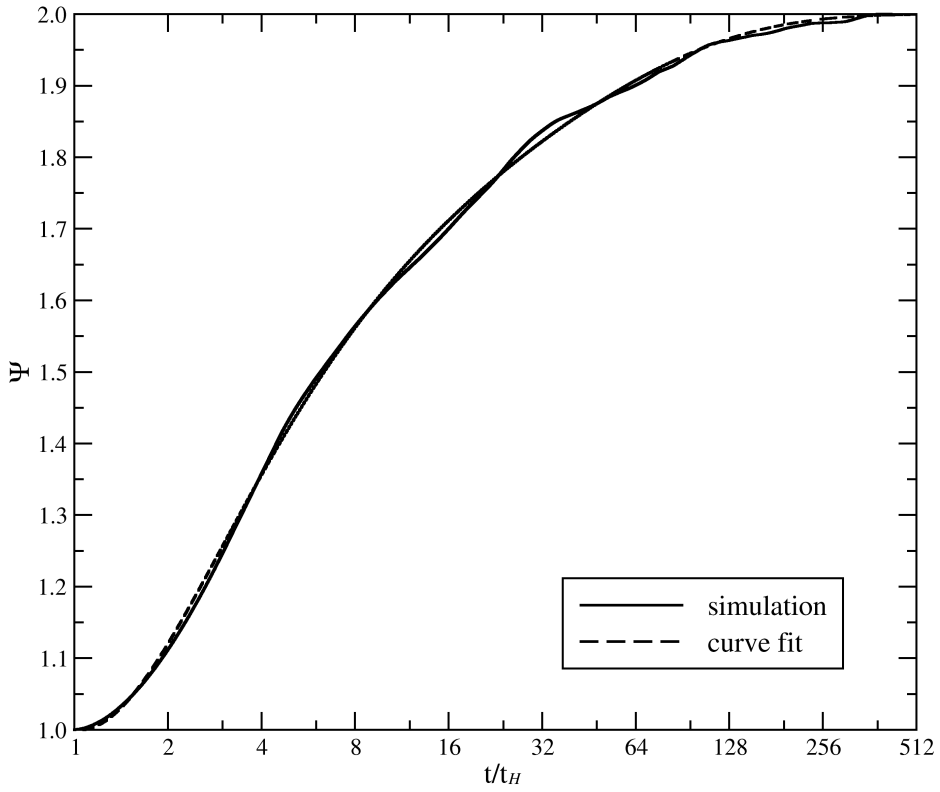

Figure 9. The reflection function, $\Psi = (V_H/V)^{5/2}(t/t_H)^3 \approx 2 - \exp(0.0269291\tau - 0.374597\tau^2 + 0.108919\tau^3 - 0.0128575\tau^4)$, where $\tau \equiv \ln(t/t_H)$.

5. Conclusions

A universal reflection function exists for ideal blasts rebounding from perfect surfaces. We have computed this function from numerical simulations of Taylor blast waves with different yields, heights of burst and ambient air densities. The reflection function relates nondimensional blast volume to nondimensional time, causing all cases to collapse onto a single curve. This curve serves as the basis for estimating the yield of tower shots and other nuclear events, wherein the cameras recorded the expanding blast wave after the shock reached the ground. Using the theory presented in this paper, it is possible to reconcile the EG&G data for Mohawk; i.e., if the reflection function is included in the blast wave analysis then the yield comes into agreement with the light-curve data and both methods give ~ 248 kilotons. In Part II of this series, we will extend this theory to include real-gas effects, humidity, gravity and energy-absorbing surfaces.

Acknowledgements. This work was performed under the auspices of the U.S. Department of Energy by Lawrence Livermore National Laboratory under Contract DE-AC52-07NA27344 and was supported by the LLNL-LDRD Program under Project Nos. 20-SI-006 and 18-ERD-049. Additional support was provided by the NNSA NA-11 Mission Effectiveness Program.

References

1 G. I. Taylor. The formation of a blast wave by a very intense explosion I. Theoretical discussion. *Proc. Roy. Soc. London, Ser. A*, 201:159–174, 1950.
2 G. I. Taylor. The formation of a blast wave by a very intense explosion. II. The atomic explosion of 1945. *Proc. Roy. Soc. London, Ser. A*, 201:175–187, 1950.
3 J. von Neumann and R. D. Richtmyer. A method for the numerical calculations of hydrodynamical shocks. *J. Appl. Phys.*, 21:232–237, 1950.
4 L. I. Sedov. *Similarity and Dimensional methods in Mechanics, Fourth Ed.* Academic Press, New York, 1959.
5 S. Tang and Wang. Q. D. Supernova blast waves in low-density hot media: A mechanism for spatially distributed heating. *The Astrophysical Journal*, 628:205–209, 2005.
6 R. Weaver, R. McCray, and J. Castor. Interstellar bubbles. ii. structure and evolution. *The Astrophysical Journal*, 218:377–395, 1977.
7 J. P. Ostriker and C. F. McKee. Astrophysical blastwaves. *Reviews of Modern Physics*, 60:1–68, 1988.
8 F. K. Shu. *The Physics of Astrophysics, Volume II, Gas Dynamics*. University Science Books, 1992.
9 U.S. Department of Energy. United States Nuclear Tests July 1945 through September 1992. DOE/NV–209-REV 16, September 2015.
10 R. E. Jackson. Guide to U.S. Atmospheric Nuclear Weapon Effects Data. Defense Nuclear Agency Technical Report: AD-B178 624 (DASIAC SR-92-007), 1993.
11 E. P. O'Connell. Teapot Apple and Redwing Mowhawk fireball asymmetries and jets. Edgerton, Germeshausen & Grier, Inc., Technical Memorandum No. B-30, 1957.
12 M. DeRosa, F. Famá, M.A. Harith, V. Palleschi, A. Salvetti, D.P. Singh, M. Vaselli, E.M. Barkudarov, M.O. Mdivnishvili, I.V. Sokolov, and M.I. Taktakishvili. Mach reflection phenomenon in the interaction of spherical shock waves in air. *Phys. Lett. A*, 156:89–95, 1991.
13 A. W. Cook and J. J. Riley. Direct numerical simulation of a turbulent reactive plume on a parallel computer. *J. Comput. Phys.*, 129:263–283, 1996.
14 L. Euler. Principes généraux du mouvement des fluides. *Mémoires de l'académie des sciences de Berlin*, 11:274–315, 1757.
15 S. K. Lele. Compact finite difference schemes with spectral-like resolution. *J. Comput. Phys.*, 103:16–42, 1992.
16 A. W. Cook and W. H. Cabot. A high-wavenumber viscosity for high-resolution numerical methods. *J. Comput. Phys.*, 195:594–601, 2004.

17 A. W. Cook and W. H. Cabot. Hyperviscosity for schock-turbulence interactions. *J. Comput. Phys.*, 203:379–385, 2005.
18 A. W. Cook. Effects of heat conduction on artificial viscosity methods for shock capturing. *J. Comput. Phys.*, 255:48–52, 2013.
19 A. W. Cook. Artificial fluid properties for large-eddy simulation of compressible turbulent mixing. *Phys. Fluids*, 19:055103, 2007.